

PARTICLE EFFECTS ON THE EXTINCTION AND IGNITION OF FLAMES IN NORMAL- AND MICRO-GRAVITY

M.G. ANDAC, F. N. EGOLFOPOULOS & C. S. CAMPBELL

Department of Aerospace & Mechanical Engineering

University of Southern California

Los Angeles, California 90089-1453

INTRODUCTION

Reacting dusty flows have been studied to lesser extent than pure gas phase flows and sprays. Particles can significantly alter the ignition, burning and extinction characteristics of the gas phase due to the dynamic, thermal, and chemical couplings between the phases. The understanding of two-phase flows can be attained in stagnation flow configurations, which have been used to study spray combustion [e.g. 1] as well as reacting dusty flows [e.g. 2]. The thermal coupling between inert particles and a gas, as well as the effect of gravity, were studied in Ref. 3. It was also shown that the gravity can substantially affect parameters such as the particle velocity, number density, mass flux, and temperature.

In Refs. 4 and 5, the effects of inert particles on the extinction of strained premixed and non-premixed flames were studied both experimentally and numerically at 1-g and μ -g. It was shown that large particles can cool flames more effectively than smaller particles. The effects of flame configuration and particle injection orientation were also addressed. It was shown that it was not possible to obtain a simple and still meaningful scaling that captured all the pertinent physics due to the complexity of the couplings between parameters. Also, the cooling by particles is more profound in the absence of gravity as gravity works to reduce the particle number density in the neighborhood of the flame.

The efforts were recently shifted towards the understanding of the effects of combustible particles on extinction [6], the gas-phase ignition by hot particle injection [7], and the hot gas ignition of flames in the presence of particles that are not hot enough to ignite the gas phase by themselves.

EXPERIMENTAL APPROACH

The experimental configuration includes the use of two counter-flowing jets in 1-g and μ -g. Particles are fed into the flow by using a particle seeder located in the bottom jet. However, the particle pickup is strongly affected by gravitational forces so that the seeder has to be calibrated separately at the lab for 1-g and on board KC-135 for μ -g. Extinction studies were conducted numerically and experimentally with 50- μ m combustible glassy-carbon particles. Premixed and non-premixed flame extinction experiments were conducted by varying the particle number density, the equivalence ratio, fuel type, flame configuration, and strain rate.

In all studies, a single flame was established at conditions close to the extinction state, below the gas phase stagnation plane (GSP) by injecting the combustible mixture from the bottom burner with the particles against an air jet. The fuel flow rate was then decreased very slowly, until the flames were extinguished. The final composition was recorded as the extinction

equivalence ratio, ϕ_{ext} , for the prevailing conditions. The strain rates were determined globally. Ignition studies were only performed numerically using 60 and 70- μm Al_2O_3 particles.

NUMERICAL APPROACH

The code was built around a quasi-one-dimensional set of equations for the gas phase similar to the one in [8], by incorporating terms that account for both the dynamic and thermal interactions between the phases. The equations for the particle phase were formulated for a single inert particle, as the number densities are small enough so that particles are unlikely to interact with each other. The code also includes a conservation equation describing the evolution of the particle number density [3]. The solutions are obtained by simultaneously integrating the entire system of equations. The kinetics was described by the GRI 3.0 mechanism [9]. The code is integrated with the CHEMKIN [10] and Transport [11] subroutine libraries.

SUMMARY OF RECENT RESEARCH

The calibration results for carbon particles are shown in Fig. 1 as the variation of injection particle number density, $n_{p,\text{inj}}$ with the gas flow rate. It can be observed that for both 1-g and μg , and for both low and high feeder speeds, n_p increases up to a certain flow rate, where it exhibits a local maximum. Above this flow rate, the rate of increase of the amount of particles put in the flow per unit time is smaller than the rate of increase in gas volume flow rate. As might be expected, n_p also increases with the particle feeder speed. The higher the feeder speed, the higher the gas flow rate corresponding to the maximum n_p is reached. More particles are entrained in the flow in μg compared to 1-g at lower flow rates but the amount of particle delivery is the same at higher flow rates regardless of gravity.

Figure 2a depicts the variation of experimentally determined ϕ_{ext} with the global strain rate K_{glb} , in 1-g for CH_4/air flames for injection number density of $n_{p,\text{inj}} \approx 0$ and $400 \text{ part}/\text{cm}^3$. In both cases ϕ_{ext} increases with K_{glb} , which should be expected as stronger flames are extinguished at larger strain rates. The data reveals that the presence of reacting carbon particles augments the resistance to extinction as weaker flames can be sustained at the same K_{glb} . The results of Fig. 2a also reveal that for high K_{glb} 's the observed difference between the ϕ_{ext} 's obtained with and without particles nearly disappears implying that the particles either do not ignite or even if they do, the ignition occurs well downstream of the gaseous flame so that the effect of the additional heat release has only a small effect on the flame.

Figure 2b depicts similar results for $\text{C}_3\text{H}_8/\text{air}$ flames. Similar to the CH_4 flames, particles appear to resist extinction at the lower K_{glb} 's, but at higher strain rates, the two curves merge and cross each other. Thus, at high strain rates, the particles do not ignite and promote extinction in exactly the same manner as inert particles.

Figure 3 depicts the opposite problem of ignition in the presence of inert particles. It shows the variation of the ignition temperature, T_{ign} , with the injection particle number density, $n_{p,\text{inj}}$, for three cases, where 60- μm Al_2O_3 particles are injected at 300 K. In all cases, particles are injected with a 1/3 molar ratio CH_4/N_2 mixture against air. Then, the temperatures of the fuel-side, the air-side or both sides were increased until ignition is achieved.

It is seen that the addition of cold particles into the flowfield significantly affects the ignition temperature for all cases regardless of whether the particles are injected from the hot or cold jet. It is also apparent that much higher temperatures are required for ignition when the air is injected cold compared to other cases. This is solely due to the strong dependence of the ignition process on OH radical generation through the main chain branching reaction $\text{H} + \text{O}_2 \rightarrow \text{OH} + \text{O}$. This reaction favors high temperatures and, as the O_2 is only available on the air-side, it will be strongly inhibited by cold air injection.

Looking at the hot air cases, ignition temperatures are smaller if the fuel and particles are initially heated - as would be expected. At first glance it appears that the two curves are parallel, but actually, there is a much weaker effect for the hot-fuel/hot-air case. Note that the two curves are 100 K apart at $n_{p,\text{inj}} = 10 \text{ part/cm}^3$ and 200 K apart at $n_{p,\text{inj}} = 1000 \text{ part/cm}^3$. Figure 4 depicts the gas phase temperature profiles for $n_{p,\text{inj}} = 10$ and 1000 part/cm^3 for the two cases right before ignition. For hot fuel, the cold particles cool the gas phase such that the temperatures around GSP are reduced dramatically. Similarly for the cold-fuel case, the location of the rapid temperature rise shifts towards the top burner, again due to the cooling by the particles.

Figure 5 depicts the H radical mass fraction distributions that also serve as markers of the ignition kernels. The results reveal that when the number density is low, the flame tries to ignite very close to the GSP on the air-side, where strain rates are highest. However, the radical pool is larger in magnitude and volume for the case that the temperatures of both jets are increased. The cooling around the GSP shifts the location of the ignition kernels towards the top burner, i.e. to lower strain rate region, but more so for the case for which the temperatures of both jets are increased. Thus, ignition becomes easier for this case compared to the other as $n_{p,\text{inj}}$ increases.

Figure 6 depicts the variation of the maximum H mass fraction, $Y_{\text{H,max}}$, with $n_{p,\text{inj}}$ for cases where premixed twin CH_4/air flames are ignited by hot 70- μm Al_2O_3 particles for three values of the equivalence ratio. The H radical increases rapidly at the ignition point. It is seen that leaner mixtures ignite easier, as indicated by the lower values of $n_{p,\text{inj}}$ and $T_{\text{max,ign}}$ found as ϕ decreases.

REFERENCES

1. Chen, G. & Gomez, A., *Proc. Combust. Inst.* **24**: 1531-1539 (1992).
2. Gomez, A. & Rosner, D.E., *Combust. Sci. Tech.* **89**: 335-362 (1993).
3. Egolfopoulos, F.N. & Campbell, C.S., *Combust. Flame* **117**: 206-226 (1999).
4. Andac, M.G., Egolfopoulos, F.N., Campbell, C.S. & Lauvergne, R., *Proc. Combust. Inst.* **28**: 2921-2929 (2000).
5. Andac, M.G., Egolfopoulos, F.N. & Campbell, C.S., *Combust. Flame*, **129**:179-191 (2001).
6. Andac, M.G., Egolfopoulos, F.N. & Campbell, C.S., *Proc. Combust. Inst.* **29**, in press.
7. F. N. Egolfopoulos, C.S. Campbell, and M.G. Andac, *Proc. Combust. Inst.* **29**, in press.
8. Bowman, C.T., Frenklach, M., Gardiner, W.R., and Smith, G. 1999 "The GRI 3.0 Chemical Kinetic Mechanism." http://www.me.berkeley.edu/gri_mech/.
9. Kee, R. J., Miller, J. A., Evans, G. H. & Dixon-Lewis, G., *Proc. Combust. Inst.* **22**: 1479-1494 (1988).
10. Kee, R. J., Warnatz, J. & Miller, J. A., Sandia Report SAND83-8209, 1983.
11. Kee, R. J., Rupley, F. M. & Miller, J. A., Sandia Report SAND89-8009, 1989.

ACKNOWLEDGMENTS

This work is supported by NASA Grant NCC3-834 under the technical supervision of Dr. Ming-Shin Wu of the Glenn Research Center

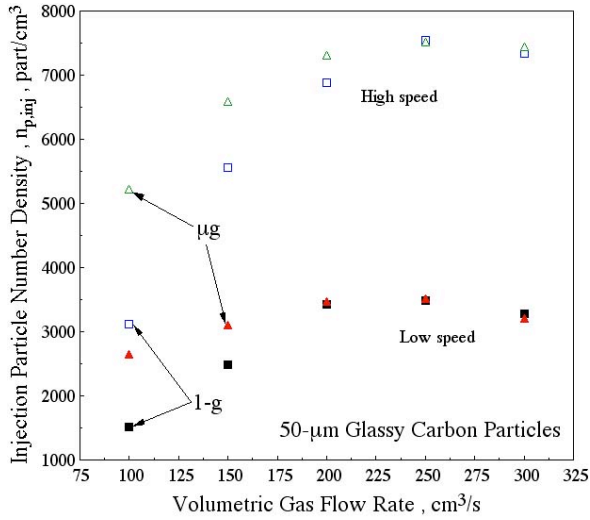


Figure 1

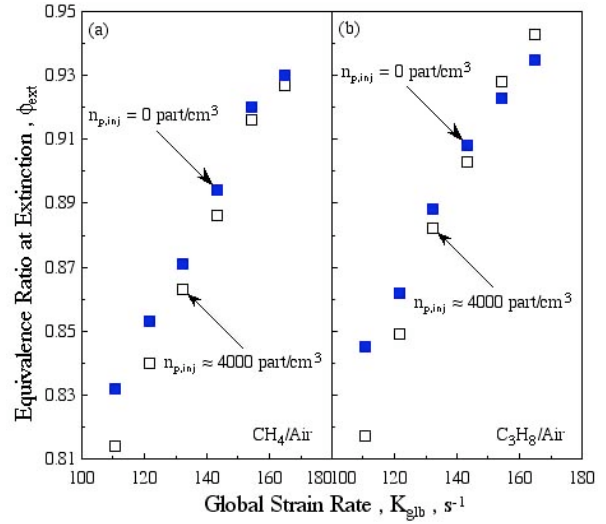


Figure 2

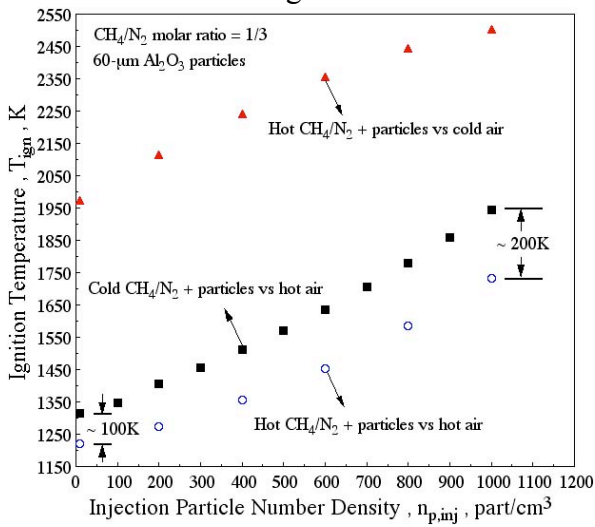


Figure 3

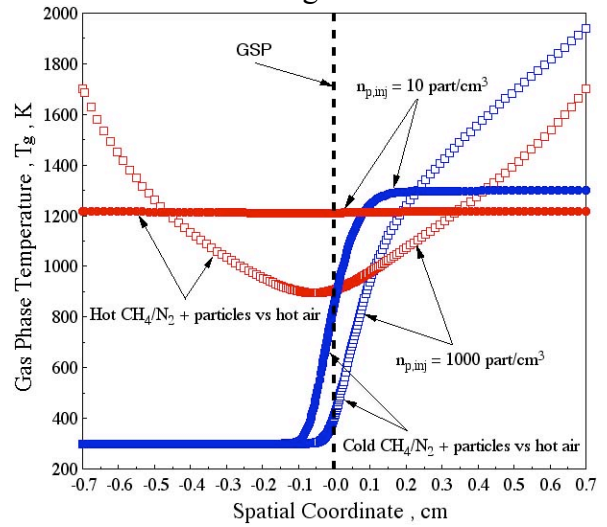


Figure 4

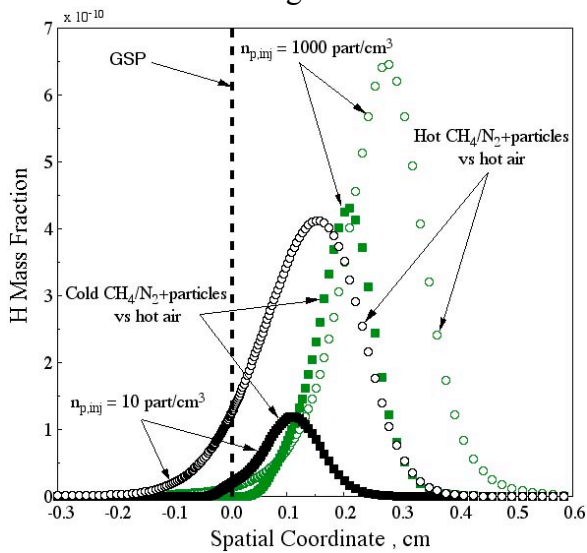


Figure 5

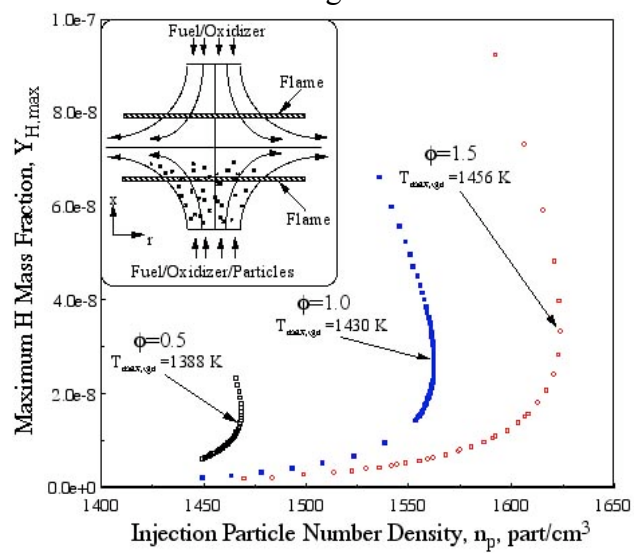


Figure 6